Experiment-based thermal micromagnetic simulations of the magnetization reversal for ns-range clocked nanomagnetic logic

Grazvydas Ziemys, Stephan Breitkreutz-v. Gamm, Gyorgy Csaba, Doris Schmitt-Landsiedel, and Markus Becherer

Citation: AIP Advances **7**, 056625 (2017); doi: 10.1063/1.4974021
View online: https://doi.org/10.1063/1.4974021
View Table of Contents: http://aip.scitation.org/toc/adv/7/5
Published by the American Institute of Physics

Experiment-based thermal micromagnetic simulations of the magnetization reversal for ns-range clocked nanomagnetic logic

Grazvydas Ziemys,[1,a] Stephan Breitkreutz-v. Gamm,[1] Gyorgy Csaba,[2] Doris Schmitt-Landsiedel,[1] and Markus Becherer[3]
[1]*Institute for Technical Electronics, Technical University of Munich (TUM), Arcisstr. 21, 80333 Munich, Germany*
[2]*University of Notre Dame, 275 Fitzpatrick Hall, Notre Dame, Indiana 46556, USA*
[3]*Institute for Nanoelectronics, Technical University of Munich (TUM), Arcisstr. 21, 80333 Munich, Germany*

(Presented 1 November 2016; received 23 September 2016; accepted 25 October 2016; published online 10 January 2017)

Extensive thermal micromagnetic simulations, based on experimental data and parameters, were performed to investigate the magnetization reversal in Co/Pt nanomagnets with locally reduced perpendicular anisotropy on the nanosecond range. The simulations were supported by experimental data gained on manufactured Co/Pt nanomagnets, as used in nanomagnetic logic. It is known that magnetization reversal is governed by two mechanisms. At pulse lengths longer than 100 ns, thermal activation dominates the magnetization reversal processes and follows the common accepted Arrhenius law. For pulse lengths shorter than 100 ns, the dynamic reversal dominates. With the help of thermal micro-magnetic simulations we found out that the point where the both mechanisms meet is determined by the damping constant α of the multilayer film stack. The optimization of ferromagnetic multilayer film stacks enables higher clocking rates with lower power consumption and, therefore, further improve the performance of pNML. [http://dx.doi.org/10.1063/1.4974021]

I. INTRODUCTION

As scaling of CMOS technology becomes more challenging and extraordinary expensive, new approaches, and even new data processing paradigms, are needed to satisfy the ever growing demand for more computing resources and functionality at low price and low power. One of the most mature and experimentally proven "Beyond CMOS" technologies is Nanomagnetic Logic with perpendicular anisotropy (pNML) which is listed in the latest International Technology Roadmap for Semiconductors 2015 in the "Beyond CMOS" technology section.[1] The biggest merits of pNML technology are its ultra low power consumption, radiation hardness, non-volatility, inherent pipelining, monolithic 3D integration and much less complex interconnects.[1–3] Furthermore, the fabrication process is fully compatible with standard CMOS technology processes. This enables pNML to be considered as More than Moore (MtM) technology for it can be integrated at the CMOS's back-end-of-line (BEOL) manufacturing technology, combing the best of both worlds. Such heterogeneous integration of multiple functionality and technologies on the same chip, or at least in the same package, is considered to pave the way to satisfy the modern demand of information processing and overcoming the CMOS scaling barrier. In recent years this trend is increasingly obvious, for example, in the mobile segment. First, there are several dies integrated in one package - system in Package (SiP), and second, several functional units, such as CPU, GPU, video codecs, RF connectivity, image signal processor are also

[a]g.ziemys@tum.de

being integrated in the same chip resulting in System on chip (SoC). The next natural step would be not only heterogeneous functional integration, but also heterogeneous technology integration, that is e.g. CMOS and pNML on the same chip, such as coprocessor for pattern matching in live incoming sensors' data.

The feasibility of pNML on a device and system level has already been proven experimentally. Fabricated and fully functional inverters, majority gates and a system based on interconnected basic devices was published in recent years.[4] E. g., the experimentally shown full adder requires just five nanomagnets[5] compared to several tens of transistors in CMOS technology. The 3D nature of stray magnetic fields also enables very dense 3D integration through stacking functional layers as shown experimentally for magnetic vias and a 3D majority gate.[6,7] The CMOS compatibility with pNML is supported by the physical compact models integrated in industry standard CMOS design flow tools from "Cadence".[8]

II. pNML TECHNOLOGY

The pNML technology is based on magnetically coupled bistable nonvolatile nanomagnets structured in ultra-thin multilayer films. The magnetization vector is perpendicular to the magnets surface and encodes the Boolean logic states, i.e. pointing out upwards denotes logical '1' and downwards '0'. Logic operations are carried out by majority gates. The superposition of the input magnets' stray fields acts on the magnetic soft spot on the output magnet and determine the output magnet's state.[4] The output magnet changes it's state only at the presence of a clocking field and stray fields superposition of the inputs. An oscillating magnetic field, perpendicular to the magnets' surface acts as a clocking signal and provides the required energy for magnetic state reversal. Such field is generated by on chip structured coils near the magnets.[3] The soft spot of a magnet is called artificial nucleation center (ANC), and is generated by local irradiation with a focused ion beam (FIB). The ions locally intermix the layers of the film stack which results in a reduced magnetic anisotropy at the irradiated area. The ANC is the point where the domain is nucleated and then it spreads over the whole magnet.[9–11]

In this paper we investigated the magnetization reversal behavior at an ANC assisted by an external field by thermal micromagnetic simulations.

III. THERMAL MICROMAGNETIC SIMULATIONS

In previous work, we presented experimental data of the switching behavior of a fabricated Co/Pt magnets.[12] Results indicated two different mechanisms involved in magnetization reversal depending on the applied external field pulse length. For pulse widths longer than 100 ns, the coercivity of a magnet followed the commonly accepted Arrhenius law. At pulse widths shorter then 100 ns, a steep increase in the field amplitude needed to switch the magnet was observed. Literature suggest that this behavior originates from two different mechanisms involved for magnetization reversal.[13] To analyze and prove this observation, we now used object oriented micromagnetic framework (OOMMF) to create the thermal micromagnetic simulations that would be as realistic as possible.[14]

To reproduce the temperature effect the "theta evolver" developed at Hamburg university[15] was applied. The "theta evolver" introduces the temperature as an additional parameter in the simulations, by altering a standard Landau-Lifshitz (LL) equation into a stochastic differential equation of the Langevin type[15,16] (Eq. 2). This is done by adding a fluctuating field $\vec{h}_{fluct}$ in addition to the effective external magnetic field $\vec{H}_{eff}$. The fluctuating field is modeled as a white noise with no correlation in time, space or axis direction with it's variance calculated according to Eq. 3.[15]

$$\frac{d\vec{M}}{dt} = -|\gamma_L|\left[\vec{M}\times\vec{H}_{eff}\right] - \frac{|\gamma_L|\,\alpha}{M}\vec{M}\times\left(\vec{M}\times\vec{H}_{eff}\right) \tag{1}$$

$$\frac{d\vec{M}}{dt} = -|\gamma_L|\,\vec{M}\times\left(\vec{H}_{eff}+\vec{h}_{fluct}\right) - \frac{|\gamma_L|\,\alpha}{M}\vec{M}\times\left(\vec{M}\times\left[\vec{H}_{eff}+\vec{h}_{fluct}\right]\right) \tag{2}$$

$$Var_{\vec{h}_{fluct}} = \frac{\alpha}{1+\alpha^2} \cdot \frac{2k_B T}{\gamma_L \mu_0 M_s V} \tag{3}$$

A. High damping simulations

Extensive thermal simulations with parameter variations suggest that the steep increase of the coercive field of a magnet in the experiment at sub-100 ns pulses originates from the high damping constant. To set high damping in the simulations, precise parameters need to be chosen. The standard Landau-Lifshitz equation is only appropriate for low damping. For that reason this section explains the measures taken to ensure consistent results of high damping thermal simulations.

The first term in Landau-Lifshitz (LL) Eq. 1 describes precessional rotation of magnetization M with frequency $\omega = -\gamma H_{eff}$. The second term expresses the magnetization rotation towards the direction of the effective field, and suggests that the precession eventually stops.[17] In 1955, Gilbert pointed out that the magnetization M will actually accelerate when α increases and, therefore, can be only used for small damping. In order to address this issue, Gilbert and Kelley[18,19] proposed an alternative equation:

$$\frac{d\vec{M}}{dt} = \gamma_G \left[\vec{M} \times \vec{H}_{eff}\right] + \frac{\alpha}{\vec{M}} \vec{M} \left[\vec{M} \times \frac{d\vec{M}}{dt}\right] \tag{4}$$

By replacing the right side of the Eq. 4 with the Gilbert equation itself, the Landau-Lifshitz-Gilbert equation is obtained. This allows to compare the Landau-Lifshitz and the Gilbert equations. Both equations are similar, except for the precessional and the damping terms (see Eq. 1 and Eq. 5).

$$\frac{d\vec{M}}{dt} = \frac{\gamma_G}{1+\alpha^2} \left[\vec{M} \times \vec{H}_{eff}\right] + \frac{\alpha\gamma_G}{1+\alpha^2 M} \left[\vec{M} \times \left[\vec{M} \times \vec{H}_{eff}\right]\right] \tag{5}$$

Eq. 5 is called Landau-Lifshitz-Gilbert equation.[17] By comparing the LL (Eq. 1) with the LLG (Eq. 5) the both parameters can be derived.

$$\gamma_L \rightarrow \frac{\gamma_G}{1+\alpha^2} \tag{6}$$

For the consistency with OOMMF and theta evolver's documentations only γ_L was used, and α_L was substituted by α_G and denoted as α. OOMMF takes as a parameter only one alpha α, however, both γ_L and γ_G. More detailed derivation is provided in Ref. 17.

B. Simulations parameters

The experiment was performed on ($Ta_{3nm}/Pt_{3nm}/4x[Co_{0.8nm}/Pt_{1.5nm}]/Pt_4$) nanomagnets of 500 nm by 3μm size. The magnet's coercivity was measured by applying magnetic field pulses of various length, ranging from 1 s to 20 ns and evaluating the magnetization by Laser-Kerr-effect microscope.[12] To reproduce the experiment by simulation several measures were taken. The most import area of a magnet for reversal is the FIB generated ANC and the surrounding area. In this area magnetization reversal starts and then spreads through the whole magnet. For simulations, a 250 nm x 250 nm region of a magnet around the ANC (50 nm x 50 nm) was chosen. Fig. 1 shows the uniaxial anisotropy profile. The anisotropy was randomly varied by 5 %. This reproduces the multilayer film stack defects and other imperfections, which results from the sputtering processes. The mean value of the uniaxial anisotropy was set to $K_u = 2.2 \times 10^5$ J/m^3, corresponding to 81 % of the experimentally measured value. The anisotropy at the ANC was set to 40% of the not irradiated area ($K_{u,anc} = 0.88 \times 10^5$ J/m^3). The 19 % deviation of used anisotropy for simulations, could originate from several sources, such as saturation magnetization M_s, assumed layer thickness, damage by FIB during the lithography or insufficient precision of anisotropy's measurements. M_s of the whole magnetic film stack is set to 5.8×10^5 A/m.

To ensure that the simulation of a small part of an experimentally characterized magnet does not influence the simulation results, a simulation of the full area of a magnetic island was performed to extract the field which act on the area of interest. The extracted field vector is applied as bias field for further thermal simulations. This is necessary to reduce the overall simulation time as several ten-thousands of simulations are required. Moreover, for each simulation the sample is initialized with a relaxed magnetization state, extracted from relaxation step simulation, to ensure the correct

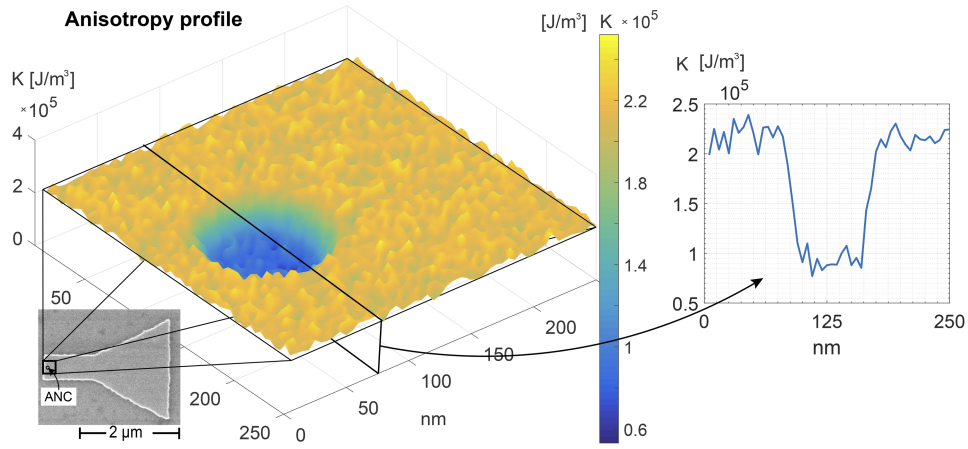

FIG. 1. Anisotropy profile with an ANC of a simulated part of a nanomagnet. Inlet shows an SEM image of a fabricated magnet which was used for the experiment. The circle in the inlet shows a 50 x 50 nm FIB irradiation area.

magnetization time evolution. Finally, the simulations were parallel distributed to the 250 CPUs threads using GNU Linux tool *Parallel.*[20]

C. Results and discussion

To obtain an Arrhenius curve, one hundred simulations were performed at 36 different field values from 150 to 500 Oe in 10 Oe steps. Overall simulation time was set to 1.2 μs and led to 3500 total simulations with one parameter set. Then the magnetization was evaluated and the number of reversals in each time interval was counted. This leads to the Arrhenius curves depicted in Fig. 2. Evaluation of a field value at 50% for each curve in Arrhenius plot gives the so-called 'Sharrock plot' and is depicted in Fig. 3 a). Fig. 3 a) describes a switching probability of a magnet in dependence of applied pulse width. The orange dots denote the experimental data on a real magnet, while the yellow line shows the calibrated thermal simulations' results. Moreover, the solid blue line is a fitted Sharrock curve to the experimental data. While the experiment, Sharrock fit and the simulations are in a very good agreement for the long pulse widths (longer than 100 ns), for the shorter pulse widths (below 100 ns), the experimental data deviates from the Sharrock curve considerably. To reproduce the steep increase of the field amplitude needed to switch a magnet as observed in the experiment,[12] parameters, especially the damping constant α and the exchange constant A_{ex} of the OOMMF simulations were varied. It turns out that the key parameter, which determines the point where the steep increase of the magnetic field starts, is the magnetic film's damping constant α. The impact of α is investigated by varying only the damping constant α, in the range from 0.5 to 50, while keeping other parameters constant. The simulations' results of α variations are presented in Fig. 3 b). Fig. 3 c) shows how the damping constant α impacts the time needed to revers the magnetization of a magnetic island at 300 Oe. The time needed to switch the magnet shows linear dependency on the damping constant.

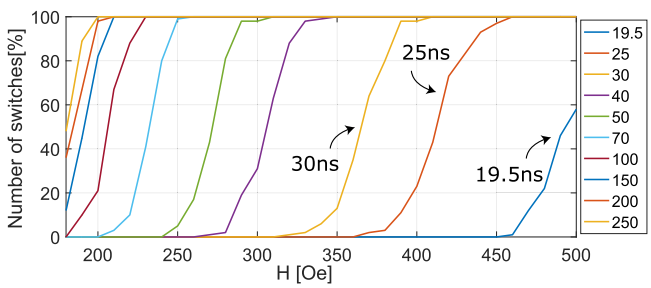

FIG. 2. Arrhenius curves obtained by OOMMF simulations of 250 by 250 nm magnet with ANC. Each line shows the probability of switching at particular external magnetic field during given pulse width.

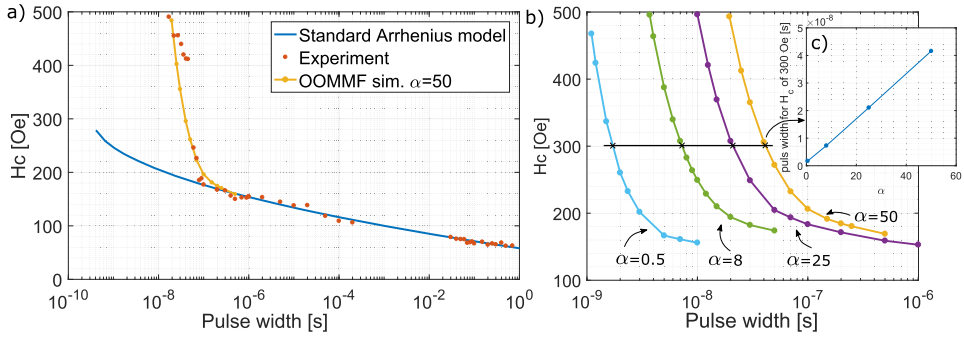

FIG. 3. a) Coercivity of the investigated magnet as function of the field pulse width (t_p). The orange dots show the measurement data while the blue solid line illustrates the commonly applied Sharrock equation to model the coercivity. The yellow solid line depicts the thermal OOMMF simulations with high damping constant α. b) Coercivity of a magnet for different α values. The curves were obtained by varying only the damping constant α (from 0.5 to 50) while keeping other parameters constant. c) Depicts pulse width required to switch the magnet at 300 Oe for different alpha values.

Choosing an α of 50 leads to the simulation's results very close to the experiment on the fabricated magnet, as can be observed in Fig. 3 a). The simulation's curve matches both switching regimes. For longer pulse widths the curve follows the Arrhenius fit and for sub-100 ns pulse widths it reproduces the dynamic magnetization reversal.

IV. CONCLUSIONS

This work presents a realistic thermal micromagnetic simulations, calibrated according to the experimental data and measurements. The key result is that the magnetic film damping constant α determines a steep increase point, where the thermally governed magnetization reversal mechanism is overtaken by the temperature independent dynamic switching process. This is especially important for optimizing magnetic film stacks for pNML. The steep increase point (see Fig. 3 a)) should be shifted far to the left, in order to allow higher clocking rates at lower power. This could be probably achieved by employing Co/Ni, film stacks with Dzyaloshinskii-Moriya Interaction (DMI) or optimizing sputtering processes.

ACKNOWLEDGMENTS

The authors would like to thank the DFG (Grant Nr. SCHM 1478/9-2 and SCHM 1478/11-1) for financial support.

[1] "The International technology roadmap for semiconductors (ITRS 2.0): Beyond CMOS," (2015).
[2] J. Hutchby, "The nanoelectronics roadmap," in *Emerging Nanoelectronic Devices* (John Wiley & Sons Ltd, 2014) pp. 1–14.
[3] M. Becherer, J. Kiermaier, S. Breitkreutz, I. Eichwald, G. Žiemys, G. Csaba, and D. Schmitt-Landsiedel, "Towards on-chip clocking of perpendicular nanomagnetic logic," Solid-State Electronics **102**, 46–51 (2014).
[4] S. Breitkreutz, J. Kiermaier, I. Eichwald, X. Ju, G. Csaba, D. Schmitt-Landsiedel, and M. Becherer, "Majority gate for nanomagnetic logic with perpendicular magnetic anisotropy," IEEE Transactions on Magnetics **48**, 4336–4339 (2012).
[5] S. Breitkreutz, I. Eichwald, J. Kiermaier, A. Papp, G. Csaba, M. Niemier, W. Porod, D. Schmitt-Landsiedel, and M. Becherer, "1-Bit full adder in perpendicular nanomagnetic logic using a novel 5-input majority gate," EPJ Web of Conferences **75**, 05001 (2014).
[6] I. Eichwald, S. Breitkreutz, G. Ziemys, G. Csaba, W. Porod, and M. Becherer, "Majority logic gate for 3D magnetic computing," Nanotechnology **25**, 335202 (2014).
[7] I. Eichwald, S. Breitkreutz, J. Kiermaier, G. Csaba, D. Schmitt-Landsiedel, and M. Becherer, "Signal crossing in perpendicular nanomagnetic logic," Journal of Applied Physics **115**, 17E510 (2014).
[8] G. Žiemys, A. Giebfried, M. Becherer, I. Eichwald, D. Schmitt-Landsiedel, and S. B. v. Gamm, "Modeling and simulation of nanomagnetic logic with cadence virtuoso using verilog-A," Solid-State Electronics (2016).
[9] S. Breitkreutz, J. Kiermaier, S. Vijay Karthik, G. Csaba, D. Schmitt-Landsiedel, and M. Becherer, "Controlled reversal of Co/Pt dots for nanomagnetic logic applications," Journal of Applied Physics **111**, 07A715 (2012).
[10] S. Breitkreutz, A. Fischer, S. Kaffah, S. Weigl, I. Eichwald, G. Ziemys, D. Schmitt-Landsiedel, and M. Becherer, "Time-dependent domain wall nucleation probability in field-coupled nanomagnets with perpendicular anisotropy," Journal of Applied Physics **117**, 17B503 (2015).
[11] J. H. Franken, M. Hoeijmakers, R. Lavrijsen, and H. J. M. Swagten, "Domain-wall pinning by local control of anisotropy in pt/co/pt strips," Journal of Physics: Condensed Matter **24**, 024216 (2012).

[12] G. Žiemys, C. Trummer, S. B.-v. Gamm, I. Eichwald, D. Schmitt-Landsiedel, and M. Becherer, "Characterization of the magnetization reversal of perpendicular nanomagnetic logic clocked in the ns-range," AIP Advances **6**, 056404 (2016).
[13] V. L. Safonov and H. N. Bertram, "Dynamic-thermal reversal in a fine micromagnetic grain: Time dependence of coercivity," Journal of Applied Physics **87**, 5681 (2000).
[14] M. J. Donahue, D. G. Porter, N. I. of Standards, and T. (U.S.), *OOMMF user's guide [microform]* / M. J. Donahue, D. G. Porter, version 1.0. ed. (U.S. Dept. of Commerce, Technology Administration, National Institute of Standards and Technology Gaithersburg, MD, 1999) pp. iii, 83 p.
[15] O. Lemcke, "Models finite temperature via a differential equation of the langevin type," (2015).
[16] J. L. García-Palacios and F. J. Lázaro, "Langevin-dynamics study of the dynamical properties of small magnetic particles," Phys. Rev. B **58**, 14937–14958 (1998).
[17] H. Kronmller, "General micromagnetic theory," in *Handbook of Magnetism and Advanced Magnetic Materials* (John Wiley & Sons, Ltd, 2007).
[18] T. L. Gilbert and J. Kelly, "Anomalous rotational damping in ferromagnetic sheets," in *Conf. Magnetism and Magnetic Materials, Pittsburgh, PA*, 253–263 (1955).
[19] T. L. Gilbert, "A phenomenological theory of damping in ferromagnetic materials," IEEE Transactions on Magnetics **40**, 3443–3449 (2004).
[20] O. Tange, "GNU parallel - the command-line power tool," The USENIX Magazine **36**, 42–47 (2011).